Article

Cell Metabolism

The CDP-Ethanolamine Pathway Regulates Skeletal Muscle Diacylglycerol Content and Mitochondrial Biogenesis without Altering Insulin Sensitivity

Graphical Abstract

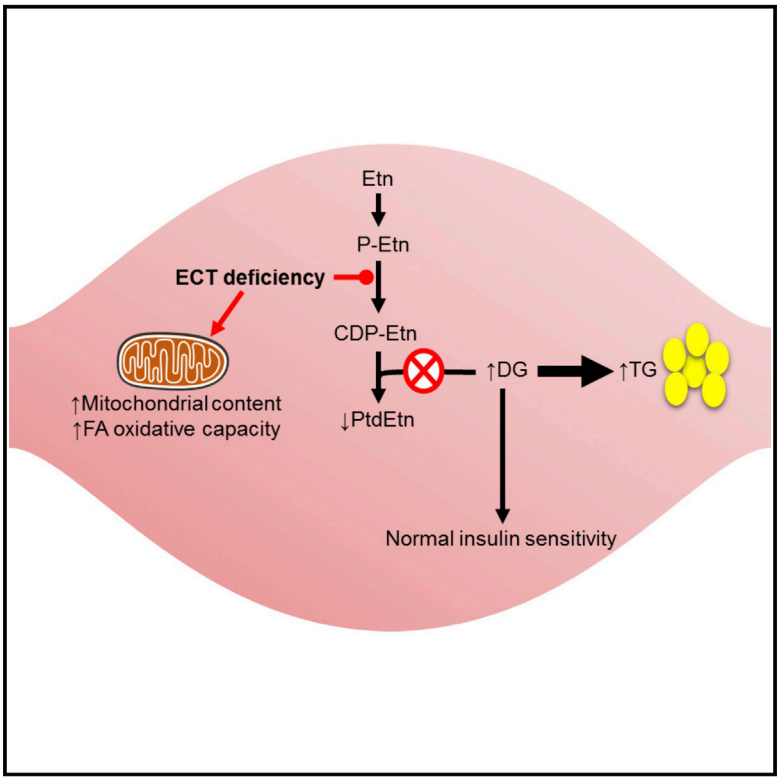

Authors

Ahrathy Selathurai, Greg M. Kowalski, ..., Mark A. Febbraio, Clinton R. Bruce

Correspondence

clinton.bruce@deakin.edu.au

In Brief

Accumulation of diacylglycerol (DAG), a phospholipid precursor, is associated with insulin resistance. Selathurai et al. show that eliminating the CDP-ethanolamine pathway in skeletal muscle causes DAG accumulation and alters membrane phospholipid composition. However, insulin sensitivity remains normal, and muscle mitochondrial content, oxidative capacity, and exercise performance are enhanced.

Highlights

- The CDP-ethanolamine pathway was eliminated from muscle
- Muscle ECT deficiency altered phospholipid species and increased diacylglycerol
- Insulin sensitivity was normal in mice lacking the CDP-ethanolamine pathway
- ECT deficiency increased mitochondrial biogenesis and oxidative capacity

Selathurai et al., 2015, Cell Metabolism *21*, 718–730
May 5, 2015
http://dx.doi.org/10.1016/j.cmet.2015.04.001

CellPress

Cell Metabolism
Article

The CDP-Ethanolamine Pathway Regulates Skeletal Muscle Diacylglycerol Content and Mitochondrial Biogenesis without Altering Insulin Sensitivity

Ahrathy Selathurai,[1,7] Greg M. Kowalski,[1,7] Micah L. Burch,[2] Patricio Sepulveda,[2] Steve Risis,[3] Robert S. Lee-Young,[3] Severine Lamon,[1] Peter J. Meikle,[4] Amanda J. Genders,[5] Sean L. McGee,[5] Matthew J. Watt,[2] Aaron P. Russell,[1] Matthew Frank,[6] Suzanne Jackowski,[6] Mark A. Febbraio,[3] and Clinton R. Bruce[1,*]

[1]Centre for Physical Activity and Nutrition (C-PAN) Research, School of Exercise and Nutrition Sciences, Deakin University, Burwood, 3125 VIC, Australia
[2]Department of Physiology, Monash University, Clayton, 3800 VIC, Australia
[3]Cellular and Molecular Metabolism Laboratory
[4]Metabolomics Laboratory
Baker IDI Heart and Diabetes Institute, Prahran, 3004 VIC, Australia
[5]Metabolic Research Unit, Deakin University, Waurn Ponds, 3216 VIC, Australia
[6]Department of Infectious Diseases, St. Jude Children's Research Hospital, Memphis, TN 38105, USA
[7]Co-first author
*Correspondence: clinton.bruce@deakin.edu.au
http://dx.doi.org/10.1016/j.cmet.2015.04.001

SUMMARY

Accumulation of diacylglycerol (DG) in muscle is thought to cause insulin resistance. DG is a precursor for phospholipids, thus phospholipid synthesis could be involved in regulating muscle DG. Little is known about the interaction between phospholipid and DG in muscle; therefore, we examined whether disrupting muscle phospholipid synthesis, specifically phosphatidylethanolamine (PtdEtn), would influence muscle DG content and insulin sensitivity. Muscle PtdEtn synthesis was disrupted by deleting CTP: phosphoethanolamine cytidylyltransferase (ECT), the rate-limiting enzyme in the CDP-ethanolamine pathway, a major route for PtdEtn production. While PtdEtn was reduced in muscle-specific ECT knockout mice, intramyocellular and membrane-associated DG was markedly increased. Importantly, however, this was not associated with insulin resistance. Unexpectedly, mitochondrial biogenesis and muscle oxidative capacity were increased in muscle-specific ECT knockout mice and were accompanied by enhanced exercise performance. These findings highlight the importance of the CDP-ethanolamine pathway in regulating muscle DG content and challenge the DG-induced insulin resistance hypothesis.

INTRODUCTION

Lipids have a crucial role in biology and are essential for maintenance of membrane integrity, enzyme function, cell signaling, and energy metabolism. However, excess tissue lipid deposition is linked to a number of pathologies, particularly insulin resistance and type 2 diabetes (Perseghin et al., 1999; Turner et al., 2013). Indeed, extensive evidence demonstrates that accumulation of triacylglycerol (TG) in skeletal muscle is associated with insulin resistance (Perseghin et al., 1999). TG itself directly interfering with insulin action is unlikely, but the general consensus is that accumulation of bioactive lipids, particularly diacylglycerol (DG), causes insulin resistance (Itani et al., 2002; Li et al., 2004; Yu et al., 2002). In addition to being an important metabolic intermediate for TG, DG is a precursor for the synthesis of phospholipids. Therefore, the DG-consuming steps of phospholipid synthesis are likely to contribute to the regulation of intramyocellular DG. However, the interaction between phospholipid and DG metabolism in skeletal muscle has not been well characterized. We therefore pursued this relationship by examining whether manipulation of phospholipid synthesis in skeletal muscle, specifically phosphatidylethanolamine (PtdEtn), would influence DG content and subsequently alter skeletal muscle insulin sensitivity.

PtdEtn is the second most abundant phospholipid in mammals (Bogdanov et al., 2008). The DG-consuming CDP-ethanolamine pathway is a major route for PtdEtn synthesis in mammalian cells (Bleijerveld et al., 2007; Sundler et al., 1974), with the rate-limiting step being the reaction catalyzed by phosphoethanolamine cytidylyltransferase (ECT). The importance of PtdEtn derived from the CDP-ethanolamine pathway is highlighted by the fact that global knockout (KO) of ECT is embryonic lethal (Fullerton et al., 2007). While PtdEtn has many important functions in cell biology (for review see Pavlovic and Bakovic, 2013; Vance and Tasseva, 2013), evidence is emerging to suggest that PtdEtn synthesis via the CDP-ethanolamine pathway is important in regulating DG levels (Leonardi et al., 2009). Specifically, hepatic deletion of ECT caused DG accumulation as well as marked liver steatosis (Leonardi et al., 2009). However, the impact of disrupting muscle PtdEtn synthesis on DG content and insulin sensitivity remains largely unexplored.

To examine this, we generated a conditional KO mouse with ECT-deficient muscle. We hypothesized that elimination of

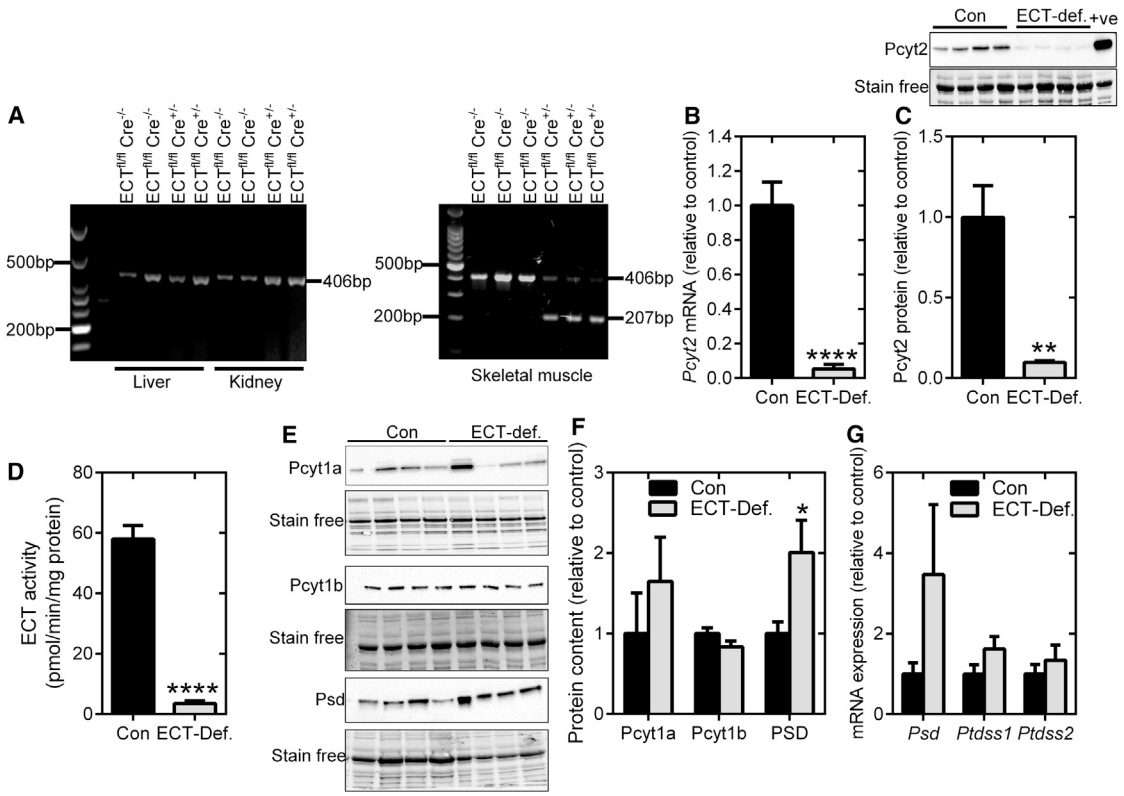

Figure 1. ECT mRNA, Protein, and Activity

(A) Genotyping of liver, kidney, and quadriceps muscle of control (*Pcyt2*$^{fl/fl}$, *Mck-Cre*$^{0/0}$) and KO mice (*Pcyt2*$^{fl/fl}$, *Mck-Cre*$^{+/0}$). Note different brands of DNA ladders were used for genotyping the liver and kidney versus skeletal muscle.

(B) *Pcyt2* mRNA in muscle from *floxed* control (n = 6) and ECT KO mice (n = 6; ECT-Def.).

(C) ECT protein in control (n = 6) and ECT-deficient muscle (n = 4).

(D) ECT activity in muscle of control (n = 9) and ECT KO mice (n = 6).

(E) Immunoblot showing protein levels of phospholipid biosynthetic enzymes.

(F) Quantification of protein levels of phospholipid biosynthetic enzymes in control (n = 4) and ECT-deficient muscle (n = 4).

(G) mRNA expression of phospholipid biosynthetic genes in control (n = 5) and ECT-deficient muscle (n = 5). Data are mean ± SEM. *p < 0.05; **p < 0.01; ****p < 0.0001.

ECT in muscle would cause a reduction in DG utilization via the CDP-ethanolamine pathway, leading to DG accumulation and muscle insulin resistance. Although the absence of ECT resulted in a dramatic increase in muscle DG, it did not cause whole-body or skeletal muscle insulin resistance. Surprisingly, however, we found that mice with ECT-deficient muscle exhibited an increase in mitochondrial biogenesis and oxidative capacity that was accompanied by enhanced endurance exercise performance. Thus, in addition to demonstrating that the CDP-ethanolamine pathway plays a significant role in controlling muscle DG levels, we have identified previously unrecognized roles for the PtdEtn in regulating muscle function and mitochondrial biology.

RESULTS

Muscle-Specific ECT KO Mice

To generate mice with ECT-deficient muscle, we ablated exon 2 from the *Pcyt2* gene, which encodes ECT, using the Cre-LoxP system (Leonardi et al., 2009). The selective deletion of *Pcyt2* in muscle was verified by genotyping muscle and a selection of other tissues (Figure 1A). Only a single band of 406 bp was detected in the liver and kidney from both the *Pcyt2*$^{fl/fl}$/*Mck-Cre*$^{0/0}$ and *Pcyt2*$^{fl/fl}$/*Mck-Cre*$^{+/0}$ mice, showing the presence of only the *floxed* ECT gene. In contrast, muscle from *Pcyt2*$^{fl/fl}$/*Mck-Cre*$^{+/0}$ mice primarily expressed the 207-bp band corresponding to removal of exon 2 from *Pcyt2* (Figure 1A). Further confirmation of the deletion of *Pcyt2* in muscle is demonstrated by the ~95% reduction in *Pcyt2* mRNA, ECT protein, and activity in *Pcyt2*$^{fl/fl}$/*Mck-Cre*$^{+/0}$ mice (Figures 1B–1D). The residual expression and activity is likely due to the presence of additional cell types other than muscle in the quadriceps (Brüning et al., 1998). We then examined whether deletion of *Pcyt2* altered the expression of enzymes in compensating pathways. The protein content of phosphocholine cytidylyltransferase (Pcyt) 1a and 1b, enzymes involved in phosphatidylcholine (PtdCho) synthesis, was not altered, while elimination of the CDP-ethanolamine pathway caused a 2-fold increase in the protein and mRNA content of phosphatidylserine decarboxylase (PSD), an alternate route for PtdEtn synthesis, which is localized to mitochondrial membranes (Figures 1E–1G). Phosphatidylserine synthase 1 (*Ptdss1*) and 2 (*Ptdss2*) mRNA expression was normal in ECT-deficient muscle (Figure 1G).

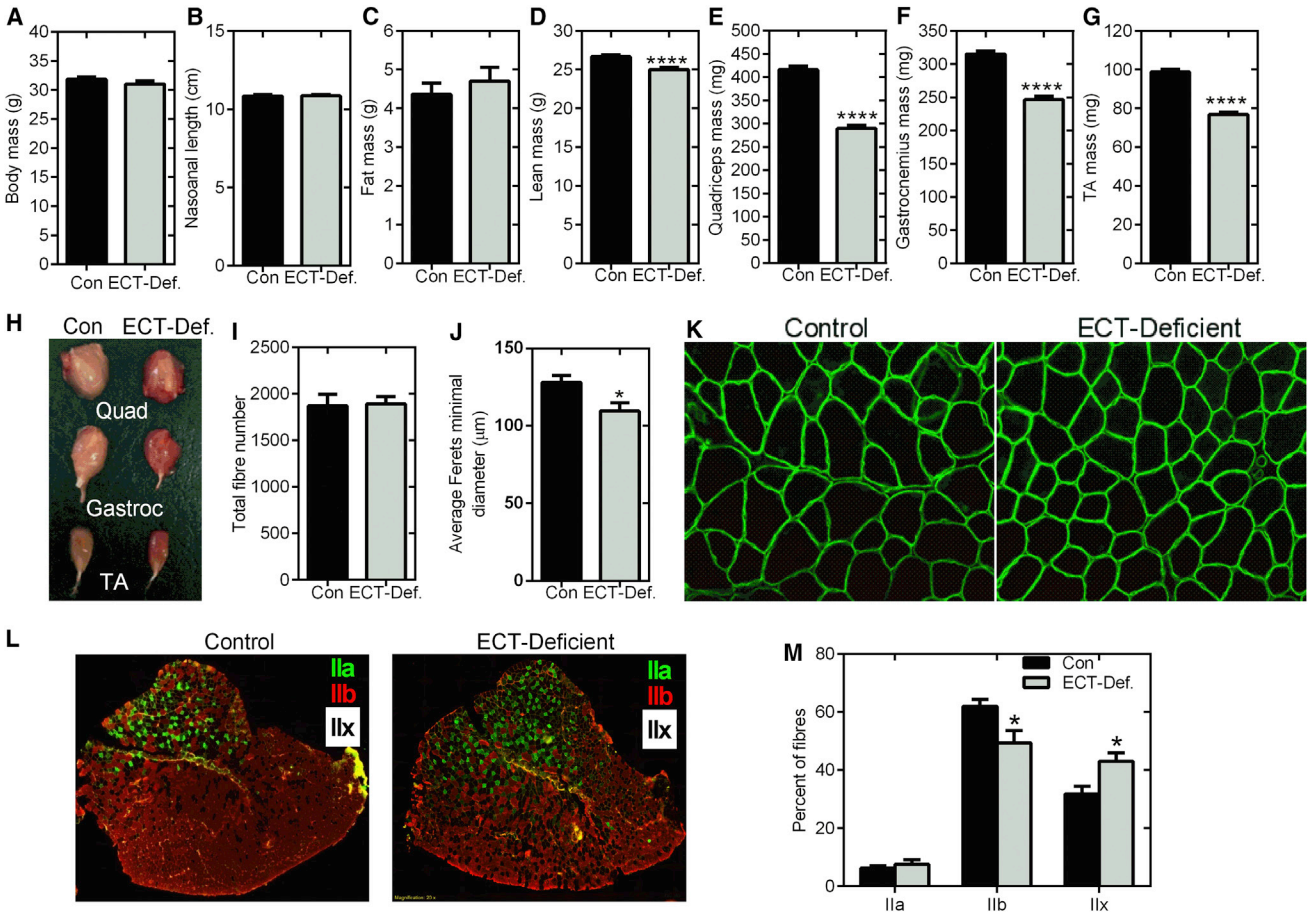

Figure 2. Body Composition of Control and Muscle-Specific ECT KO Mice

(A) Body mass (n = 56 for control; n = 52 for ECT-deficient).

(B) Naso-anal length of control (n = 11) and ECT KO mice (n = 5).

(C) Fat mass (n = 56 for control; n = 52 for ECT-deficient).

(D) Lean mass (n = 56 for control; n = 52 for ECT-deficient).

(E) Quadriceps mass (n = 47 for control; n = 36 for ECT-deficient).

(F) Gastrocnemius mass (n = 47 for control; n = 36 for ECT-deficient).

(G) Tibialis anterior (TA) mass (n = 47 for control; n = 36 for ECT-deficient).

(H) The gross appearance of muscles from control and ECT KO mice.

(I) Total fiber number in TA muscles (n = 5).

(J) Average Feret's minimal diameter of fibers from TA muscles (n = 4).

(K) Cross section of dystrophin-stained TA muscle from control and ECT KO mice (40× magnification).

(L) Representative image of TA muscle showing myosin heavy chain expression.

(M) Quantitative analysis of fiber type distribution. Data are mean ± SEM. For the individual muscle data, the combined mass of both muscles is presented. *$p < 0.05$; ****$p < 0.0001$.

General Characteristics

Muscle-specific ECT KO mice appeared outwardly normal with no change in body mass or naso-anal length (Figures 2A and 2B). While no difference in fat mass (Figure 2C) was found, lean mass was reduced in muscle-specific ECT KO mice (Figure 2D). To determine the basis of this difference, the weights of a variety of hindlimb muscles were assessed. Quadriceps, gastrocnemius, and tibialis anterior (TA) mass were all reduced by 25%–30% in ECT-deficient mice (Figures 2E–2G). Importantly, this phenotype was attributed to the loss of ECT as opposed to non-specific effects of expression of *Cre* or the *floxed Pcyt2* gene as lean mass and quadriceps mass were not different between the *floxed* control animals, *Mck-Cre* control mice ($Pcyt^{0/0}$/*Mck-Cre*$^{+/0}$), or wild-type control mice ($Pcyt^{0/0}$/*Mck-Cre*$^{0/0}$; Figures S1A and S1B). In addition to being smaller, the musculature of ECT-deficient mice had a marked increase in red coloration (Figure 2H). Histological analysis of the TA muscle revealed that the reduction in muscle mass in the ECT KO mice was not caused by changes in myofiber number (Figure 2I), but was due to a reduction in myofiber size (Figures 2J and 2K). In addition, the TA muscle from the ECT KO mice exhibited a modest shift in myosin heavy chain (MHC) isoform expression with a reduction in the number of MHCIIb fibers, and an increase in MHCIIx-expressing fibers (Figures 2L and 2M).

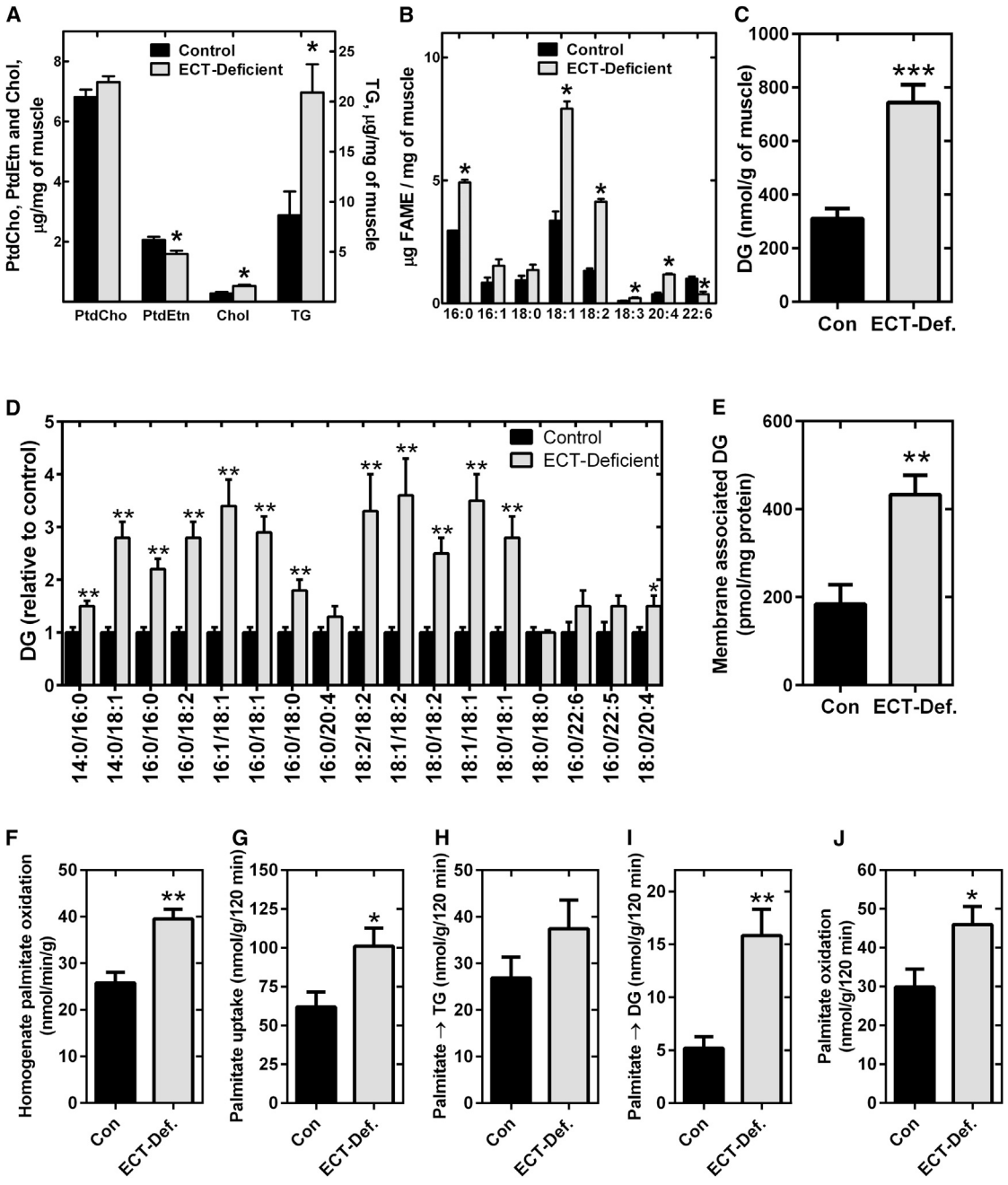

Figure 3. Lipid Handling in ECT-Deficient Muscle

(A and B) (A) Lipid content and (B) total fatty acid methyl ester (FAME) composition of control (n = 3) and ECT-deficient quadriceps muscle (n = 3).

(C) DG content in quadriceps of control (n = 6) and ECT KO mice (n = 6).

(D) DG species in control (n = 28) and ECT-deficient muscle (n = 28).

(E) Membrane-associated DG in muscle from control (n = 8) and ECT KO mice (n = 7).

(F) Palmitate oxidation in homogenates from control (n = 4) and ECT KO mice (n = 8).

(G–J) (G) Skeletal muscle palmitate uptake, (H) esterification into TG, (I) DG, and (J) oxidation (n = 7 for control; n = 11 for ECT KO). Data are mean ± SEM. *$p < 0.05$; **$p < 0.01$; ***$p < 0.001$.

Lipid Metabolism

The ECT-deficient muscles had a significant imbalance in the levels of the major lipid classes (Figure 3A). The content of PtdEtn was 22% lower than in control animals, while there was no difference in PtdCho in the KO compared with control mice (Figure 3A). Cholesterol was increased almost 90%, and TG was elevated by ~150% in the ECT-deficient muscles (Figure 3A). The overall FA composition was also different in the ECT-deficient muscle (Figure 3B), with substantial increases in 16:0, 18:1, 18:2, and 20:4, and a reduction in 22:6. In addition, total DG content was about

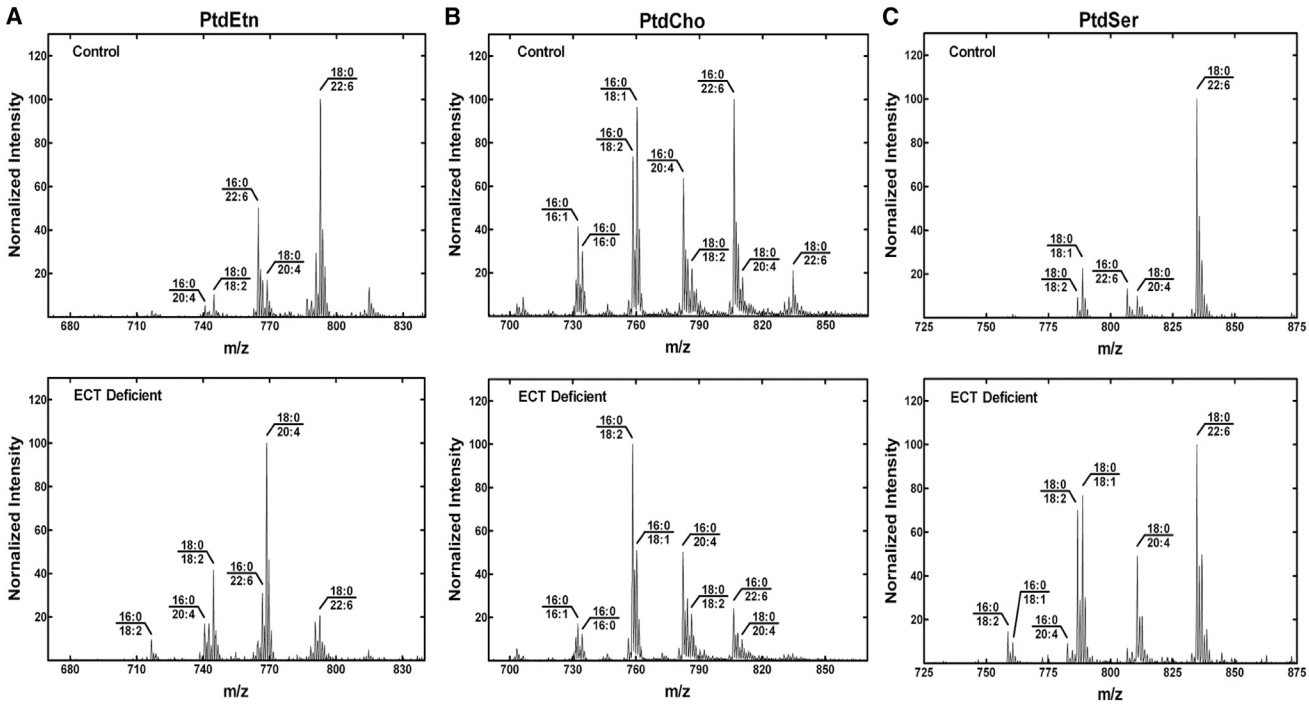

Figure 4. The Phospholipid Molecular Species Composition of ECT-Deficient Muscle

(A–C) The molecular species composition of (A) PtdEtn, (B) PtdCho, and (C) PtdSer. The molecular species fingerprints are of a typical control and ECT-deficient muscle and are representative of three mice per genotype. The identification of the primary phospholipid molecular species in each of the major peaks was based on the fatty acid composition and the preponderance of saturated fatty acids in the 1-position and unsaturated fatty acids in the 2-position of phospholipids.

2-fold higher in ECT-deficient muscle (Figure 3C). The FA composition of DG was dramatically altered in ECT-deficient muscle with 2- to 3-fold increases in 16:0-, 18:1-, and 18:2-containing DG species (Figure 3D). Furthermore, membrane-associated DG was 2-fold higher in ECT-deficient muscle (Figure 3E). The changes in lipid composition were associated with an increase in SREBP1c (*Srebf1*) mRNA, while the expression of other genes involved in lipid synthesis including *Dgat1*, *Dgat2*, *Fasn*, and *Scd1* (Figure S2A) was unchanged. Deletion of ECT also caused significant alterations in FA handling, with ECT-deficient muscle exhibiting an increase in FA oxidation in a muscle homogenate preparation (Figure 3F). Furthermore, in an intact ex vivo system, rates of FA uptake and esterification into TG and DG were elevated in ECT-deficient muscle (Figures 3G–3I). Ex vivo FA oxidation was also increased in muscle from ECT KO mice (Figure 3J), but was not associated with any change in the expression of *Cd36* or *Cpt1b* (Figure S2A). Muscle glycogen was elevated in ECT-deficient muscle (Figure S2B), consistent with observations demonstrating that when FA oxidation is increased in muscle, glucose is diverted away from glycolysis and pyruvate oxidation toward glycogen storage (Hoehn et al., 2010; Randle et al., 1963).

Phospholipid Composition

Elimination of the CDP-ethanolamine pathway and subsequent reliance on the mitochondrial PSD pathway for PtdEtn synthesis led to dramatic changes in the composition of the major phospholipids. There was a pronounced difference in the PtdEtn composition in ECT-deficient muscle (Figure 4A). (18:0/22:6) PtdEtn was the most abundant species in controls, and was almost absent in muscle from the ECT KO mice. (18:0/20:4) PtdEtn was the predominant species in the ECT-deficient muscle with lower amounts of (18:0/22:6)PtdEtn. Overall, the PtdEtn in the ECT-deficient muscle was enriched in species containing 18:0 paired with a polyunsaturated FA and deficient in species containing 16:0 paired with a polyunsaturated FA. Although there were no significant changes in the amount of PtdCho, there were differences in the PtdCho species (Figure 4B). (16:0/18:1)PtdCho and (16:0/22:6)PtdCho were the most prevalent species in the controls. In the muscle-specific ECT KO mice there was a decrease in the abundance of PtdCho molecular species containing 22:6 leading to (16:0/18:2)PtdCho becoming the most abundant species. Phosphatidylserine (PtdSer) was dominated by (18:0/22:6)PtdSer in both control and ECT-deficient muscle, constituting about 80% of PtdSer in controls, but only about 30% in ECT-deficient muscle (Figure 4C). In addition, the notable difference in the PtdSer pool in muscle of the ECT KO mice was a higher level of species with 16:0. These findings demonstrate that inactivation of the CDP-ethanolamine pathway in muscle not only influences the composition of PtdEtn, but also has a major impact on the molecular species of PtdCho and PtdSer.

Mitochondrial Content Is Increased in ECT-Deficient Muscle

The increased red coloration of the ECT-deficient muscle together with the elevated rates of FA oxidation suggest that mitochondrial content is increased in muscle from ECT KO

mice. Indeed, electron microscopy (Figure 5A) demonstrated an increase in mitochondrial density in the KO mice. Furthermore, the expression of complexes II and V of the electron transport chain (Figure 5B) as well as the intensity of succinate dehydrogenase (SDH) staining (Figure 5C) was elevated in ECT-deficient muscle. We therefore examined whether mitochondrial biogenesis was increased by determining mitochondrial protein synthesis in vivo using heavy water (^2H_2O) labeling. Body water enrichment of ^2H_2O (Figure S2C) remained constant at ~6% over the 4-week labeling period. The ECT KO mice exhibited an increase in mitochondrial protein synthesis (Figure 5D), demonstrating that the increase in mitochondrial content was due to enhanced mitochondrial biogenesis. Consistent with these findings, cardiolipin, a mitochondrial-specific lipid, was increased in ECT-deficient muscle (Figure 5E), as were citrate synthase and β-HAD activity (Figures 5F and 5G). Mitofusion 2 and PINK1 protein levels were not changed (Figure S2E), suggesting that alterations in mitochondrial fusion or mitophagy were not responsible for the increase in mitochondrial content in ECT-deficient muscle. We next examined whether this was associated with changes in known regulators of mitochondrial biogenesis. The activity of AMP kinase (AMPK) was not affected by ECT deletion (Figure S2D), nor were the protein levels of PGC1α or cytochrome c oxidase subunit IV (COX4; Figure 3H). However, mitochondrial transcription factor A (TFAM) protein was ~70% higher in ECT-deficient muscle (Figure 3H). Interestingly, the mRNA expression of PGC1α (*Ppargc1a*), *Tfam*, and *Cox4* were actually reduced by ~50% in ECT-deficient muscle (Figure S2A). In contrast, mitochondrial fission 1 protein (*Fis1*) was increased, while PGC1β (*Ppargc1b*), PPARα (*Ppara*), PPARδ (*Ppard*), and mitofusin 2 (*Mfn2*) were not altered (Figure S2A). A link between PtdEtn and calcium homeostasis in muscle has been reported (Funai et al., 2013), and given that activation of calcium signaling has been associated with mitochondrial biogenesis, the phosphorylation status of calcium/calmodulin-dependent protein kinase II (CaMKII) was examined. No differences in CaMKII protein or phosphorylation were found between control and ECT-deficient muscle (Figure S2F). As DG can activate protein kinase D (PKD) 1 (Sundram et al., 2011), a serine-threonine kinase that when overexpressed drives an oxidative phenotype in muscle (Kim et al., 2008), we examined whether the increased mitochondrial content in ECT-deficient muscle could be related to DG-induced activation of PKD1. However, PKD1 phosphorylation was reduced in ECT KO mice, which appeared to be due to a corresponding reduction in total PKD1 protein (Figure S2G); thus, the ratio of phosphorylated-to-total PKD1 remained unchanged. Functionally, the increase in mitochondrial content in ECT-deficient muscle was associated with enhanced respiratory capacity as shown by an increase in oxygen consumption rates in the presence of complex I and II substrates (Figure 5I). Furthermore, endurance exercise capacity was enhanced in ECT KO mice (Figure 5J). We next investigated whether the increased FA oxidative capacity of ECT-deficient muscle would influence whole-body substrate utilization during exercise. Oxygen consumption was similar between genotypes (Figure 5K), but the RER was lower in the muscle-specific ECT KO mice demonstrating an increased reliance on fat oxidation during exercise (Figure 5L). Elimination of the CDP-ethanolamine pathway also had a significant impact on the mitochondrial phospholipid profile (Figure S4). Similar to whole muscle, (18:0/22:6)PtdEtn was the most abundant species in mitochondria from control muscle, but was dramatically reduced in mitochondria from ECT-deficient muscle. The most predominant PtdEtn species in mitochondria from ECT-deficient muscle were (18:0/18:2) and (18:0/20:4)PtdEtn. In addition, mitochondria from the ECT KO mice contained a larger proportion of PtdEtn containing 16:0 and 18:0 FAs. In contrast, the mitochondrial PtdCho profile was similar between control and ECT-deficient mice. Interestingly, PtdCho in mitochondria from both the control and ECT KO mice was found to be lacking in polyunsaturated FAs.

Energy Expenditure and Insulin Sensitivity Are Normal in Muscle-Specific ECT KO Mice

Despite the increase in muscle oxidative capacity in ECT KO mice, whole-body oxygen consumption, substrate utilization, and food intake were similar to control animals (Figures 6A–6C). In addition, physical activity levels were comparable between the control and ECT KO mice, ruling out the possibility that the increase in mitochondria was due to changes in activity levels (Figure 6D). To determine whether the increase in muscle lipid content, as well as the changes in the composition of the phospholipids in ECT-deficient muscle, was associated with altered insulin sensitivity, euglycemic hyperinsulinemic clamps were performed. Glucose levels were matched in both strains and were clamped at basal levels (Figure 6E). The glucose infusion rate was identical between strains (Figure 6F) as were the plasma insulin levels under fasting and clamp conditions (Figure 6G), demonstrating that insulin sensitivity was not impaired in ECT KO mice. Endogenous glucose production under basal and clamped conditions was not different between strains (Figures 6H and 6I), and as such, percent suppression of endogenous glucose production was similar (85% ± 9% versus 72% ± 7% for control and muscle-specific ECT KO mice, respectively; $p > 0.05$). Deletion of ECT from muscle had no effect on peripheral glucose disposal (Figure 6J) or muscle glucose uptake (Figures 6K and 6L). Accumulation of lipids, specifically DG, is proposed to cause muscle insulin resistance via activation of protein kinase (PKC) θ (Griffin et al., 1999; Kim et al., 2004). Despite elevated DG in ECT-deficient muscle, we failed to detect any change in membrane-bound PKCθ or its phosphorylation status (Figure S4). Plasma free fatty acids (FFAs) were lower in the ECT KO compared with the control mice prior to clamp, and were suppressed to levels observed in control mice under clamp conditions (Figure 6M). Thus, despite marked lipid accumulation and striking alterations in the phospholipid composition, insulin sensitivity was preserved in ECT-deficient muscle.

Muscle Lipid Content and Oxidative Capacity Are Not Altered by ECT Overexpression

To determine whether overexpression of ECT alters muscle lipids and oxidative capacity, a recombinant AAV6 vector expressing ECT was administered systemically to C57Bl/6 mice. As expected, ECT protein and activity in quadriceps muscle were increased, while there was no effect in liver and adipose tissue (Figures S5A and S5B). Despite the increase in ECT activity, there was no change in body mass, quadriceps mass,

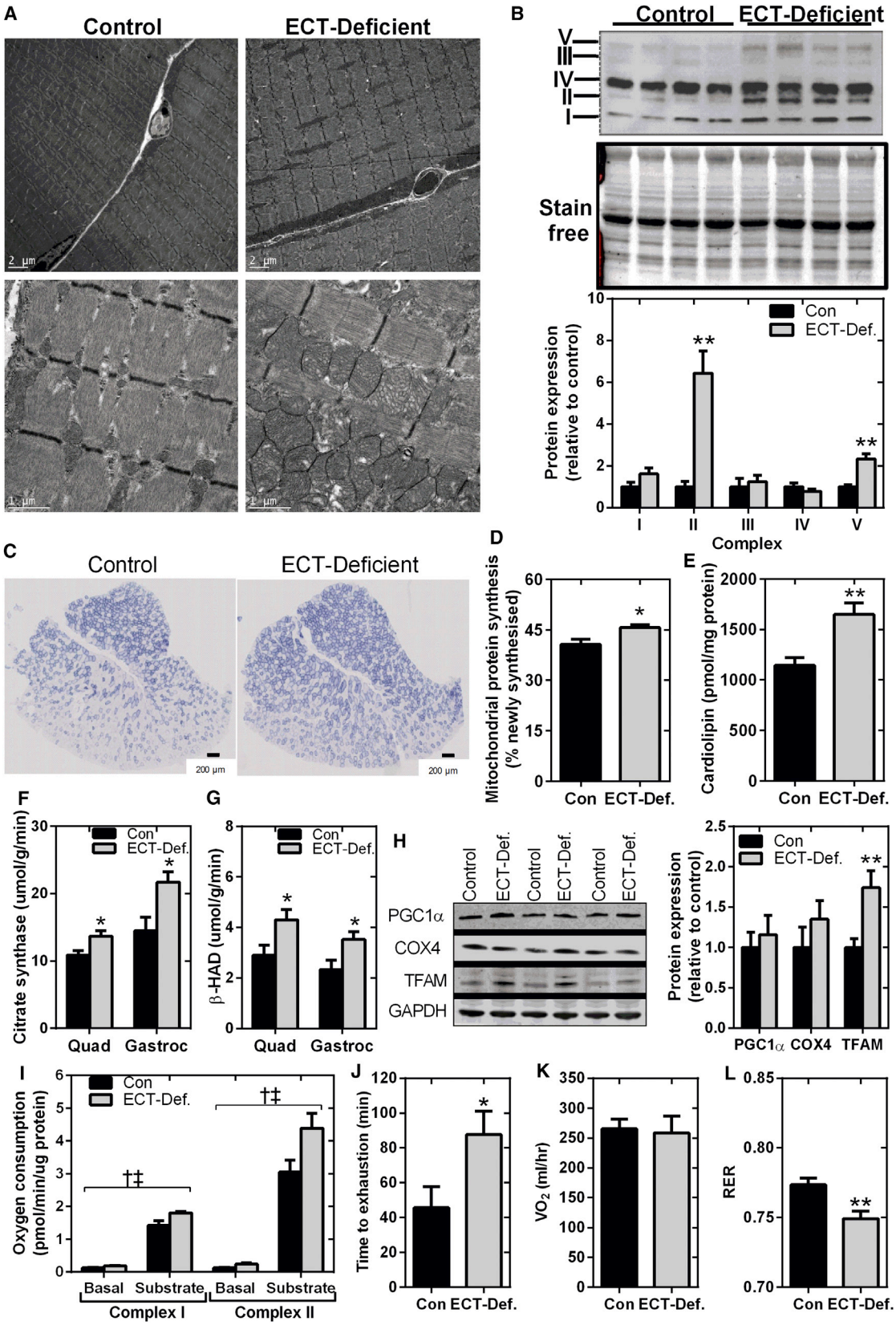

(legend on next page)

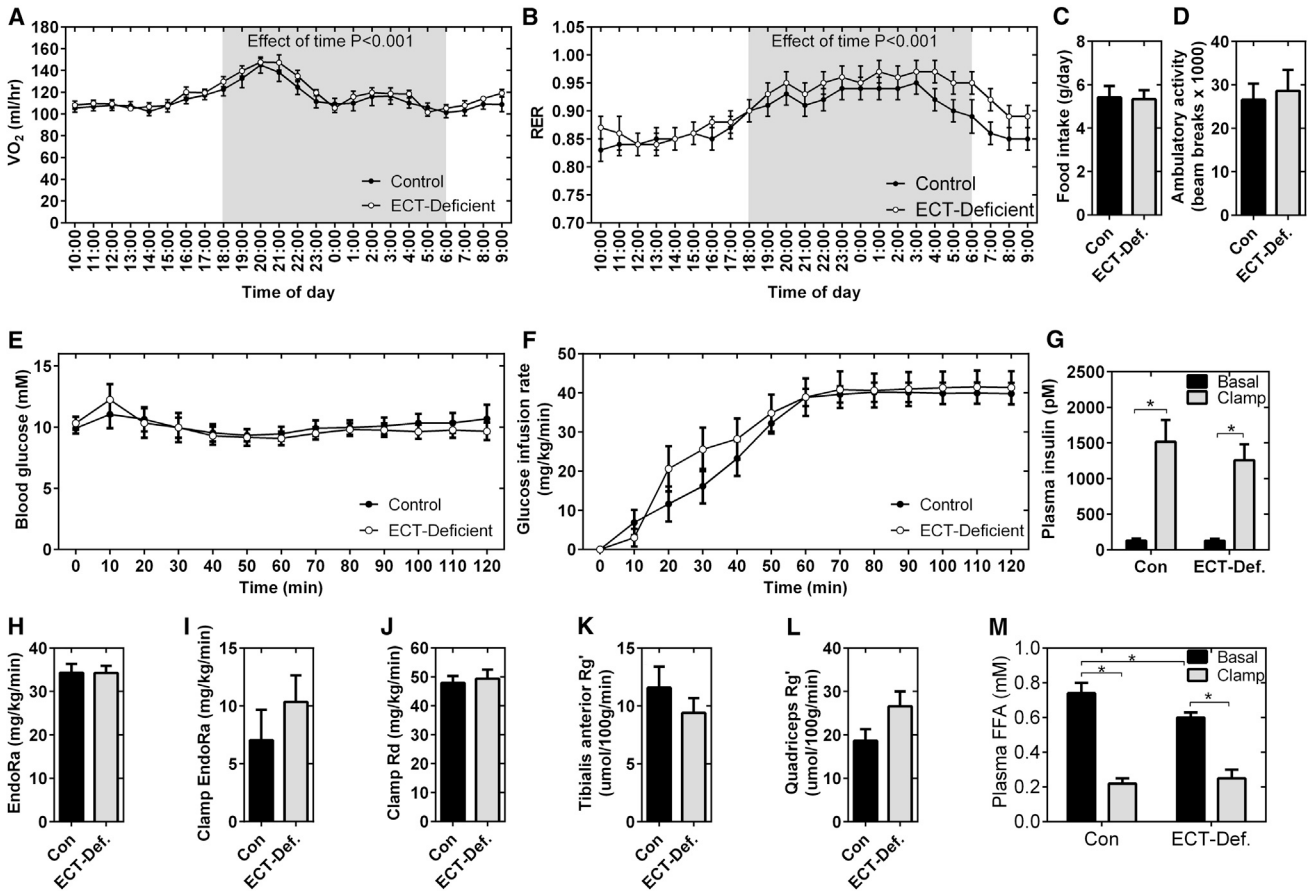

Figure 6. Energy Metabolism and Insulin Sensitivity in Muscle-Specific ECT KO Mice

(A–D) (A) VO_2, (B) RER, (C) 24-hr food intake, and (D) physical activity levels (n = 12 per group). The dark phase is represented by the shaded area.

(E and F) (E) Blood glucose levels and (F) glucose infusion rates during the euglycemic hyperinsulinemic clamp.

(G) Plasma insulin prior to and at the end of the clamp.

(H and I) (H) The endogenous rate of appearance (EndoRa) of glucose under basal and (I) clamp conditions.

(J) The rate of glucose disappearance (Rd) during the euglycemic hyperinsulinemic clamp.

(K and L) (K) Glucose uptake into the TA and (L) quadriceps muscle.

(M) Basal and clamp FFA levels. Data are mean ± SEM. For clamp data, n = 12 for control; n = 15 for ECT-deficient. *p < 0.05.

muscle lipid content, or oxidative enzyme activity (Figures S5C–S5H).

Muscle-Specific ECT KO Mice Are Not Protected against Diet-Induced Obesity and Glucose Intolerance

It has been suggested that enhanced muscle oxidative capacity may protect against the development of lipid-induced insulin resistance (Phielix et al., 2012). We therefore placed control and ECT KO mice on a high-fat diet (HFD) and examined their metabolic responses. Body mass, weight gain, and fat mass were identical in control and ECT-deficient mice in response to 4 weeks of the HFD (Figures 7A–7E). Muscle TG (4-fold) and DG (2-fold) were elevated in ECT-deficient muscle (Figures 7F and 7G), as were FA oxidation rates (Figure 7H) and citrate

Figure 5. Mitochondrial Biogenesis and Oxidative Capacity Are Increased in ECT-Deficient Muscle

(A) Electron micrograph of extensor digitorum longus muscle from control and ECT KO mice.

(B) The expression of oxidative phosphorylation proteins in Complex I–V of the electron transport chain (n = 4 for both genotypes).

(C) SDH staining of cross-sections from TA muscle of control and ECT KO mice.

(D) Mitochondrial protein synthesis (n = 9 for control; n = 5 for ECT KO).

(E) Cardiolipin content (n = 28 per group).

(F and G) (F) Citrate synthase and (G) β-HAD activity in quadriceps (Quad; n = 19 per group) and gastrocnemius (Gastroc; n = 15 per group).

(H) Representative immunoblot and quantitation of PGC1α, COX4, and TFAM protein (n = 8 per group).

(I) Basal and substrate-driven oxygen consumption rates in muscle from control (n = 12) and ECT KO mice (n = 8).

(J) Endurance exercise capacity in control (n = 6) and muscle-specific ECT KO mice (n = 8).

(K and L) (K) VO_2 and (L) RER during exercise (n = 6 per group). Data are mean ± SEM. *p < 0.05; **p < 0.01. †main effect for genotype p < 0.05; ‡main effect for substrate p < 0.05.

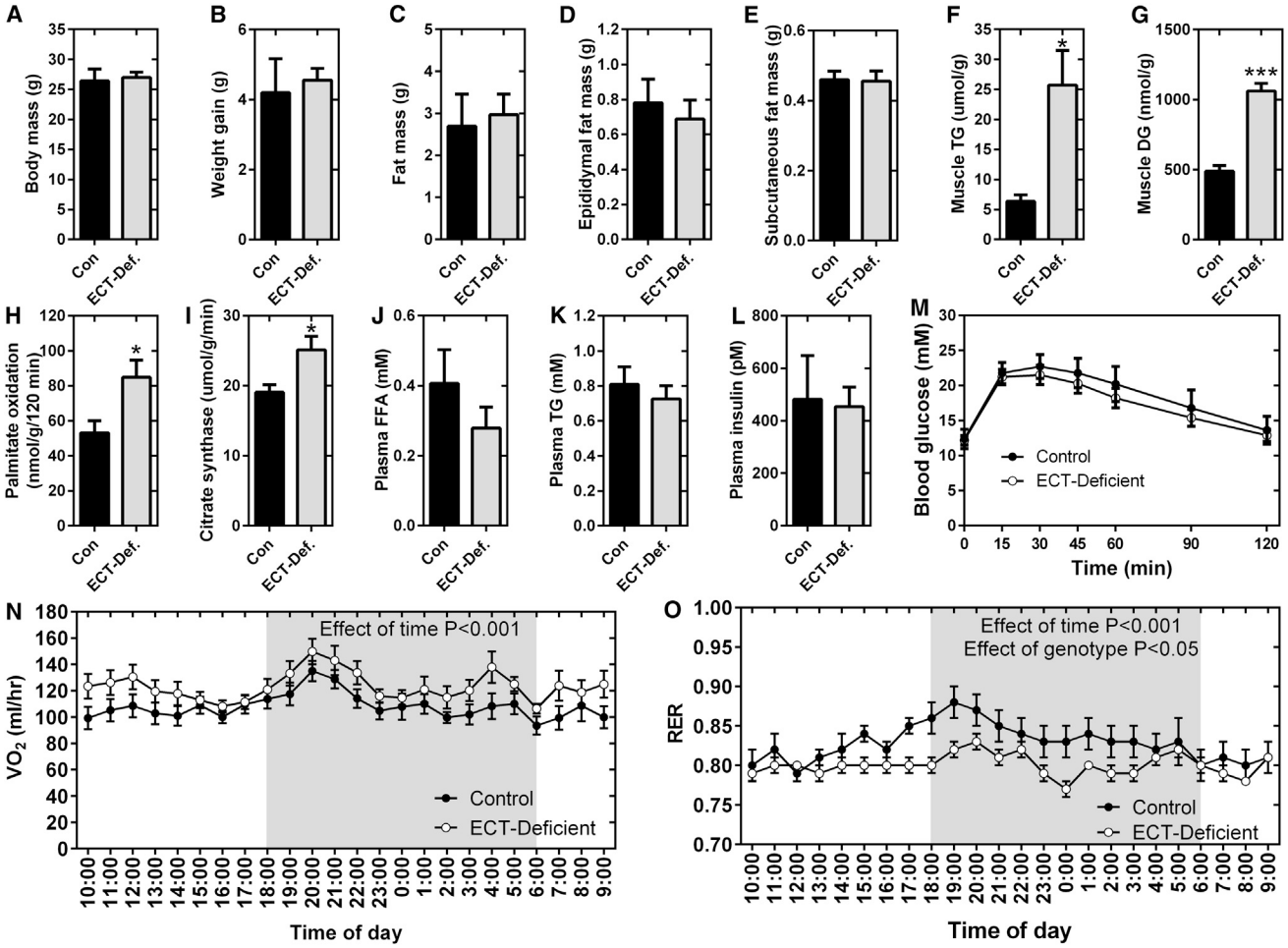

Figure 7. The Effect of a HFD on Metabolic Responses in Muscle-Specific ECT KO Mice

(A–E) Control and muscle-specific ECT KO mice were fed a HFD for 4 weeks, and body mass (A), weight gain (B), fat mass (C), and epididymal (D) and subcutaneous (E) fat mass were determined.

(F and G) Muscle TG (F) and DG (G) content were determined.

(H) Palmitate oxidation rates were determined in isolated extensor digitorum longus muscles ex vivo.

(I) Citrate synthase activity in the quadriceps muscle.

(J–L) Plasma FFA (J), triglyceride (K), and insulin (L) levels.

(M) Blood glucose levels following a glucose tolerance test.

(N and O) VO_2 (N) and RER (O). The dark phase is represented by the shaded area. Control n = 5; muscle-specific ECT KO n = 9. Data are mean ± SEM. *p < 0.05; ***p < 0.001.

synthase activity (Figure 7I). However, FFAs, triglycerides, and insulin were not different between control and ECT KO mice (Figures 7J–7L). Even though ECT-deficient muscle exhibited marked lipid accumulation, glucose tolerance was similar in ECT KO and control mice when maintained on a HFD (Figure 7M). While whole-body oxygen consumption was not different between genotypes (Figure 7N), RER was lower in the ECT KO mice demonstrating that the rates of whole-body fat oxidation were higher compared with control mice (Figure 7O). We also examined whether ECT protein levels would be affected by consumption of a HFD; however, the HFD had no effect (Figure S6). Collectively, these observations show that despite the fact that ECT-deficient mice display increased FA oxidation, they are not protected from HFD-induced muscle lipid accumulation or weight gain.

DISCUSSION

The CDP-ethanolamine pathway has emerged as an important regulator of hepatic lipid homeostasis (Fullerton et al., 2009; Leonardi et al., 2009); however, its role in skeletal muscle had not been studied. Our data provide novel and compelling evidence that the CDP-ethanolamine pathway plays a critical role in regulating muscle lipid homeostasis. ECT-deficient muscle was characterized by marked DG and TG accumulation and significant alterations in phospholipid composition, but these changes did not alter whole-body or muscle insulin sensitivity. In addition, elimination of the CDP-ethanolamine pathway in muscle had a number of surprising and unanticipated effects. The muscle-specific ECT KO mice exhibited smaller muscles that had increased mitochondrial content. This was

associated with enhanced skeletal muscle oxidative capacity and improved endurance performance. These findings highlight important, yet unexpected, roles of the CDP-ethanolamine pathway in regulating muscle function and substrate metabolism.

The absence of PtdEtn synthesis via the CDP-ethanolamine pathway disrupted skeletal muscle lipid homeostasis resulting in accumulation of both TG and DG. The utilization of DG for phospholipid synthesis at the ER is reduced due to the absence of ECT expression, and, consistent with the findings in cultured cells (Jackowski et al., 2000) and ECT-deficient liver (Fullerton et al., 2009; Leonardi et al., 2009), DG is redirected to TG synthesis. The increase in DG esterification and lipid storage in ECT-deficient muscle was further facilitated by elevated rates of FA uptake. Furthermore, consistent with previous reports linking the activation of SREBP with lipid accumulation in tissues lacking the CDP-ethanolamine pathway (Leonardi et al., 2009; Lim et al., 2011), the transcript levels of SREBP were upregulated in ECT-deficient muscle that may have also contributed to the increased DG and TG content.

Lipids, especially DG, are proposed to play a key role in the development of muscle insulin resistance (Itani et al., 2002; Li et al., 2004; Perseghin et al., 1999; Yu et al., 2002). Given the changes in lipid homeostasis observed in ECT-deficient muscle, we hypothesized that ECT KO mice would develop insulin resistance via activation of the DG-sensitive PKCθ, an established mediator of lipid-induced insulin resistance in muscle (Itani et al., 2002; Li et al., 2004; Yu et al., 2002). Contrary to our hypothesis, muscle insulin sensitivity remained intact in ECT KO mice, and despite significant DG accumulation, we did not detect any change in the activation status of PKCθ. These findings challenge the prevailing view that DG accumulation is a requisite factor in the development of skeletal muscle insulin resistance (Erion and Shulman, 2010). However, the relationship between DG accumulation and insulin action is complex, demonstrated by the fact that elevated DG levels have been found in muscle of highly trained athletes who are remarkably insulin sensitive (Amati et al., 2011). Moreover, recent studies have highlighted that in addition to the total DG, other factors including subcellular localization, FA composition, as well as the type of DG stereoisomer stored (i.e., *sn*-1,2 DG, *sn*-1,3 DG, or *sn*-2,3 DG) may influence this relationship (Bergman et al., 2012; Eichmann et al., 2012). Our finding that muscle insulin sensitivity was unaffected, despite an increase in membrane-associated DG, sheds new light on this relationship and challenges the concept that muscle insulin resistance links specifically to alterations in membrane DG content. Together, these findings provide direct evidence that increases in lipid content, localization, and specific molecular species do not necessarily cause muscle insulin resistance, and that using general measures of lipid content as a surrogate readout for insulin resistance is too simplistic.

The phospholipid content and composition of ECT-deficient muscle was also altered, with ECT KO mice exhibiting perturbations in the composition of all major phospholipid pools as well as a 22% reduction in PtdEtn content. However, as the CDP-ethanolamine pathway is considered to be the major route of PtdEtn synthesis in mammals (Bleijerveld et al., 2007; Sundler et al., 1974), it is intriguing that deletion of ECT from muscle caused such a modest reduction in PtdEtn content. Thus, it seems that the PSD pathway is able to compensate for reduced PtdEtn synthesis via the CDP-ethanolamine pathway in order to maintain relatively high levels of PtdEtn in ECT-deficient muscle. Consistent with this notion, PSD protein and mRNA were increased in ECT-deficient muscle. Furthermore, PtdEtn in the control muscle largely reflects the composition of the PtdSer pool (compare Figures 4A and 4C), suggesting that the PSD pathway is the primary source for PtdEtn in muscle. However, if this were the case, one would expect a dominance of (18:0/22:6)PtdEtn in the ECT-deficient muscle as well, but the data do not support this conclusion. Comparison of the control and ECT-deficient PtdEtn profiles (Figure 4A) suggests that the (18:0/22:6)PtdEtn is replaced by an abundance of (18:0/20:4) PtdEtn when the ECT pathway is not operational. Post de novo phospholipid remodeling either by CoA-dependent acyltransferase or CoA-independent transacylase activities, together with the availability of the essential FA linoleate (18:2n-6) in the circulation, may be responsible for the abundance of (20:4)PtdEtn in the ECT-deficient muscle (for reviews see Shindou et al., 2009; Shindou and Shimizu, 2009). Linoleate is the precursor of arachidonic acid (20:4), which is liberated for eicosanoid synthesis and, if not utilized for this purpose, can accumulate in PtdEtn. These data contrast to the PtdEtn profile in ECT-deficient liver (Leonardi et al., 2009) where there is no evidence of phospholipid remodeling, and the PtdEtn pool is a clear reflection of the FA distribution in PtdSer.

The most surprising finding of the current study was the increase in mitochondrial biogenesis in ECT-deficient muscle. This was associated with an enhanced capacity for FA oxidation, reflected by an increase in muscle FA oxidation as well as whole-body rates of fat oxidation during exercise, and was coupled with an increase in endurance exercise capacity in the ECT KO mice. When placed on a HFD, ECT KO mice had elevated rates of whole-body fat oxidation; however, this did not prevent HFD-induced lipid accumulation, nor did it alter glucose tolerance. Furthermore, as the increase in muscle oxidative capacity was not associated with a change in energy expenditure, ECT-deficient mice gained weight at the same rate as control mice when fed a HFD. These findings contrast those in *Pcyt2*$^{+/-}$ mice that have an impaired ability to oxidize FAs and develop obesity and glucose intolerance (Fullerton et al., 2009). The reason for these discrepancies is not clear, but may be related to the fact that in addition to muscle, the *Pcyt2*$^{+/-}$ mice had reduced ECT activity in other important metabolic tissues, particularly the liver, which may account for divergent effects on whole-body metabolism (Fullerton et al., 2009). However, it is worth noting that, similar to our findings, liver-specific ECT KO mice did not develop obesity, despite exhibiting severe hepatic steatosis (Leonardi et al., 2009).

Despite our extensive studies examining the mechanism(s) responsible for the increase in mitochondrial biogenesis and oxidative capacity of ECT-deficient muscle, they are not completely resolved. The modest shift in MHC isoform expression from IIb to IIx in ECT-deficient muscle is likely to play some role in contributing to this phenotype as the oxidative capacity of IIx fibers is higher than that of IIb (Bloemberg and Quadrilatero, 2012). To try to understand the mechanisms responsible, we examined regulators of mitochondrial biogenesis and fiber type determination. While there was no change

in AMPK or PPAR expression, TFAM protein was increased despite the fact that PGC1α protein was unaltered. It is interesting to note, however, that while an increase in TFAM expression causes an upregulation of mitochondrial DNA copy number, it does so without increasing respiratory capacity or mitochondrial content (Ekstrand et al., 2004), suggesting that factors in addition to an increase in TFAM are likely to be involved. Recent work has identified a role for PKD1, a DG-sensitive kinase, in regulating the oxidative phenotype in muscle (Kim et al., 2008). Activation of PKD1 leads to phosphorylation and nuclear export of class II histone deacetylases, relieving repression on myocyte enhancer factor-2, which drives an oxidative phenotype (Kim et al., 2008). As DG content was increased in ECT-deficient muscle, we examined whether activation of PKD1 could contribute to the increase in oxidative capacity. Contrary to our hypothesis, the phosphorylation status of PKD1 was actually lower in ECT-deficient muscle, but this could be due to the fact that total PKD1 levels were also reduced. It is possible that the reliance on the PSD pathway as the sole route for PtdEtn synthesis in ECT-deficient muscle may play a role in mediating the increase in mitochondrial biogenesis and oxidative capacity. PSD is localized to mitochondria; therefore, the absolute dependence on this pathway in order to maintain near-normal levels of PtdEtn in muscle lacking the CDP-ethanolamine pathway may provide a stimulus to increase mitochondrial biogenesis. Such an adaptation would be expected to enhance the capacity of PtdEtn synthesis via the PSD pathway. Unfortunately, little is known about the role of the PSD pathway in mammalian biology; however, given that PSD deficiency disrupts mitochondrial function (Tasseva et al., 2013), we speculate that the upregulation of this pathway may somehow contribute to the increase in mitochondrial biogenesis and enhanced oxidative capacity of ECT-deficient muscle.

The synthesis of membrane phospholipids, including PtdEtn, is important for growth (Pavlovic and Bakovic, 2013; Tasseva et al., 2013). Indeed, depletion of mitochondrial PtdEtn caused by silencing PSD impairs cell growth (Tasseva et al., 2013). Furthermore, the *Pcyt2* gene is induced by growth factors (Zhu et al., 2008), and global elimination of ECT is embryonic lethal (Fullerton et al., 2007), providing additional evidence that the CDP-ethanolamine pathway is critical for normal growth and development. However, it is interesting to note that no growth and developmental defects have been reported in *Pcyt2*$^{+/-}$ mice (Fullerton et al., 2009), while elimination of the CDP-ethanolamine pathway in liver did not affect proliferation, differentiation, or survival of hepatocytes (Leonardi et al., 2009). In contrast, we show that muscle-specific ECT KO mice exhibit smaller fibers and have less lean mass compared with control littermates. This is an intriguing finding and suggests that the CDP-ethanolamine pathway is required for the development and maintenance of skeletal muscle mass. Further work will be required to examine the mechanisms responsible for this phenotype and to determine whether the CDP-ethanolamine pathway is disrupted in conditions associated with accelerated muscle wasting.

We have established that the CDP-ethanolamine pathway is required for the maintenance of normal muscle lipid homeostasis. Deletion of ECT not only altered the molecular species composition of the major phospholipids in muscle, but also caused marked lipid accumulation. However, contrary to our hypothesis, the increase in DG content did not influence muscle insulin sensitivity, demonstrating that accumulation of DG is not sufficient to cause muscle insulin resistance. The elimination of the CDP-ethanolamine pathway also had unexpected effects including an increase in skeletal muscle mitochondrial biogenesis and a reduction in muscle mass. These findings not only underscore the importance of the CDP-ethanolamine pathway in regulating lipid metabolism, but also reveal a new and intriguing role for PtdEtn in regulating skeletal muscle function and mitochondrial biology.

EXPERIMENTAL PROCEDURES

Animal Experiments

Mice lacking functional ECT expression in muscle were generated by crossing *Pcyt2* floxed (*Pcyt2*$^{fl/fl}$) mice with mice expressing Cre recombinase under the control of the muscle creatine kinase promoter (*Mck-Cre*) (Brüning et al., 1998). A description of the construct design and generation of *Pcyt2*$^{fl/fl}$ mice has been detailed elsewhere (Leonardi et al., 2009). *Pcyt2*$^{fl/fl}$ mice were mated with *Pcyt2*$^{fl/fl}$, *Mck-Cre*$^{+/0}$ mice, generating mice with either normal levels of ECT in muscle (*Pcyt2*$^{fl/fl}$, *Mck-Cre*$^{0/0}$) or ECT-deficient muscle (*Pcyt2*$^{fl/fl}$, *Mck-Cre*$^{+/0}$). For all experiments, floxed littermates (*Pcyt2*$^{fl/fl}$, *Mck-Cre*$^{0/0}$) were used as controls. Unless otherwise stated, all experiments were conducted on 18-week-old male mice maintained on a standard laboratory chow diet (5% calories from fat, Specialty Feeds) and housed at 22°C ± 1°C on a 12:12-hr light-dark cycle, with free access to food and water. To increase ECT activity in muscle, a recombinant AAV vector expressing ECT was administered systemically to C57Bl/6 mice (see Supplemental Experimental Procedures for more detail). For the HFD studies, 6-week-old mice were fed a HFD (42% calories from fat, Specialty Feeds) for 4 weeks. All procedures were approved by the Alfred Medical Research and Education Precinct Animal Ethics Committee and Monash Animal Research Platform Animal Ethics Committee.

Body Composition and Muscle Histology

Fat and lean mass were determined using the EchoMRI 4-in-1 (Echo Medical Systems). Mice were then anesthetized with sodium pentobarbital (60 mg/kg), naso-anal length was determined, and muscles (extensor digitorum longus [EDL], TA, gastrocnemius, and quadriceps) were dissected, weighed, frozen in liquid nitrogen, or prepared for histological analysis including electron microscopy studies (described in Supplemental Experimental Procedures).

Lipid Metabolism

Lipids were extracted using a modification of the Bligh and Dyer method (Bligh and Dyer, 1959) optimized for lipid quantitation by the LipidMaps group (Ivanova et al., 2007). The amount of each major lipid class was determined using flame-ionization mass detection (Leonardi et al., 2009). For some studies, TG content was determined biochemically using a colorimetric assay kit (Triglycerides GPO-PAP, Roche Diagnostics) (Bruce et al., 2007). Total DG was determined according to the enzymatic-radiometric methods of Preiss et al. (Preiss et al., 1986). Analysis of membrane-associated DG was performed as previously described (Bruce et al., 2009). Cardiolipin content and the molecular species of DG were determined by mass spectrometry (Bruce et al., 2012). Phospholipid molecular species fingerprints of muscle and isolated mitochondria were determined using previously described methods (Ivanova et al., 2007; Krank et al., 2007; Leonardi et al., 2009). FA metabolism was assessed in a homogenate preparation or isolated intact EDL muscles (described in Supplemental Information).

Metabolic Assessment

Glucose tolerance tests (1 g/kg lean body mass glucose i.p.) were performed in 6-hr-fasted mice. Hyperinsulinemic euglycemic clamps were performed in conscious, restrained mice as described in detail elsewhere (Bruce et al., 2012). Plasma insulin was measured by ELISA (Millipore). FFAs were measured by an enzymatic colorimetric assay (NEFA C kit; Wako Chemicals).

Plasma triglycerides were determined using a colorimetric assay kit (Triglycerides GPO-PAP, Roche Diagnostics). Oxygen consumption (VO_2), RER, and physical activity levels were determined using a 12-chamber indirect calorimeter (Oxymax series, Columbus Instruments). Respiratory parameters were measured in individual mice over a 24-hr period under a consistent environmental temperature (22°C) with ad libitum access to food and water. In vivo mitochondrial biogenesis was determined by measuring mitochondrial protein synthesis according to the methods of Miller and colleagues (Drake et al., 2013), which are detailed in the Supplemental Information. Respiratory capacity was determined in muscle biopsies using the Seahorse XF flux analyzer (detailed in Supplemental Information). Exercise capacity was determined by performing a treadmill run to exhaustion. Mice were familiarized with the treadmill (Columbus Instruments) daily for 5 days prior to the test. On the day of the test, mice were placed on the treadmill and allowed to acclimate for 15 min before running at 16 m/min until exhaustion. After 1 week, mice performed a standardized 15-min run at 16 m/min in an enclosed treadmill (Columbus Instruments) to determine VO_2 and RER by indirect calorimetry.

Enzyme Activity Assays

ECT activity was assayed using [^{14}C]phosphoethanolamine (American Radiolabeled Chemicals) as a substrate (Fullerton et al., 2007; Leonardi et al., 2009). Citrate synthase and β-HAD activity were determined using established methods (Lowry and Passonneau, 1972; Srere, 1969). AMPK activity was measured in lysates as previously described (Lee-Young et al., 2009).

Quantitative Real-Time RT-PCR

RNA was isolated from muscle using TRIzol (Invitrogen). Samples were reverse transcribed, and gene expression analysis was performed by RT-PCR using SYBR Green PCR Master Mix (Invitrogen). 18S or 36B4 were used as house-keeping genes. The primers used are detailed in Table S1. The relative quantification was calculated using the ΔΔCt method, normalizing values to littermate controls.

Western Blotting

Quadriceps muscle was lysed, and protein (40 μg) was resolved by SDS-PAGE (Bio-Rad Laboratories). After transfer to PVDF membranes, stain-free images for total proteome visualization were collected, and membranes were blocked in 5% BSA. After incubation with primary antibody (detailed in Table S2), appropriate secondary antibodies were applied, and the immunoreactive proteins were detected with enhanced chemiluminescence and quantified by densitometry. Data was normalized to the loading control obtained from the stain-free gel and was expressed as a relative change from the control group. Analysis of membrane and cytosolic PKCθ were performed as previously described (Bruce et al., 2009).

Statistics

All data are presented as mean ± SEM. Data were analyzed by unpaired Student's t test or repeated-measures factorial ANOVA where appropriate. For the ANOVA procedures, Newman-Keuls post hoc tests were used to establish differences between groups. Statistical significance was set at $p < 0.05$.

SUPPLEMENTAL INFORMATION

Supplemental Information includes six figures, two tables, and Supplemental Experimental Procedures and can be found with this article online at http://dx.doi.org/10.1016/j.cmet.2015.04.001.

AUTHOR CONTRIBUTIONS

A.S., G.M.K., M.L.B., P.S., S.R., R.S.L.-Y., S.L., A.J.G., S.L.M., M.J.W., A.P.R., M.F., S.J., and C.R.B. conducted experiments and analyzed the data. S.L.M., P.J.M., S.J., M.J.W., A.P.R., M.A.F., and C.R.B. contributed reagents, materials, and/or analytical tools and contributed to the design of the experiments. A.S., G.M.K., S.J., M.A.F., and C.R.B. wrote the paper. All authors discussed the data and commented on the manuscript before submission.

ACKNOWLEDGMENTS

We thank C. Yang and R. Kanojia for technical assistance. The MHC antibodies were obtained from the Developmental Studies Hybridoma Bank, created by the NICHD of the NIH, and maintained at The University of Iowa, Department of Biology. The authors acknowledge the facilities and scientific and technical assistance of Monash Micro Imaging, Monash University. These studies were supported by grants from the NHMRC (APP1004239 to C.R.B. and M.A.F.), NIH (GM0457370), and the American Lebanese Syrian Associated Charities (to S.J.). C.R.B. (586698), R.S.L.-Y. (APP1052573), P.J.M. (APP1042095), S.L.M. (APP1030474), M.J.W. (606460), and M.A.F. (APP1021168) have been supported by fellowships from the NHMRC.

Received: July 16, 2014
Revised: February 20, 2015
Accepted: March 28, 2015
Published: May 5, 2015

REFERENCES

Amati, F., Dubé, J.J., Alvarez-Carnero, E., Edreira, M.M., Chomentowski, P., Coen, P.M., Switzer, G.E., Bickel, P.E., Stefanovic-Racic, M., Toledo, F.G., and Goodpaster, B.H. (2011). Skeletal muscle triglycerides, diacylglycerols, and ceramides in insulin resistance: another paradox in endurance-trained athletes? Diabetes *60*, 2588–2597.

Bergman, B.C., Hunerdosse, D.M., Kerege, A., Playdon, M.C., and Perreault, L. (2012). Localisation and composition of skeletal muscle diacylglycerol predicts insulin resistance in humans. Diabetologia *55*, 1140–1150.

Bleijerveld, O.B., Brouwers, J.F., Vaandrager, A.B., Helms, J.B., and Houweling, M. (2007). The CDP-ethanolamine pathway and phosphatidylserine decarboxylation generate different phosphatidylethanolamine molecular species. J. Biol. Chem. *282*, 28362–28372.

Bligh, E.G., and Dyer, W.J. (1959). A rapid method of total lipid extraction and purification. Can. J. Biochem. Physiol. *37*, 911–917.

Bloemberg, D., and Quadrilatero, J. (2012). Rapid determination of myosin heavy chain expression in rat, mouse, and human skeletal muscle using multicolor immunofluorescence analysis. PLoS ONE *7*, e35273.

Bogdanov, M., Mileykovskaya, E., and Dowhan, W. (2008). Lipids in the assembly of membrane proteins and organization of protein supercomplexes: implications for lipid-linked disorders. Subcell. Biochem. *49*, 197–239.

Bruce, C.R., Brolin, C., Turner, N., Cleasby, M.E., van der Leij, F.R., Cooney, G.J., and Kraegen, E.W. (2007). Overexpression of carnitine palmitoyltransferase I in skeletal muscle in vivo increases fatty acid oxidation and reduces triacylglycerol esterification. Am. J. Physiol. Endocrinol. Metab. *292*, E1231–E1237.

Bruce, C.R., Hoy, A.J., Turner, N., Watt, M.J., Allen, T.L., Carpenter, K., Cooney, G.J., Febbraio, M.A., and Kraegen, E.W. (2009). Overexpression of carnitine palmitoyltransferase-1 in skeletal muscle is sufficient to enhance fatty acid oxidation and improve high-fat diet-induced insulin resistance. Diabetes *58*, 550–558.

Bruce, C.R., Risis, S., Babb, J.R., Yang, C., Kowalski, G.M., Selathurai, A., Lee-Young, R.S., Weir, J.M., Yoshioka, K., Takuwa, Y., et al. (2012). Overexpression of sphingosine kinase 1 prevents ceramide accumulation and ameliorates muscle insulin resistance in high-fat diet-fed mice. Diabetes *61*, 3148–3155.

Brüning, J.C., Michael, M.D., Winnay, J.N., Hayashi, T., Hörsch, D., Accili, D., Goodyear, L.J., and Kahn, C.R. (1998). A muscle-specific insulin receptor knockout exhibits features of the metabolic syndrome of NIDDM without altering glucose tolerance. Mol. Cell *2*, 559–569.

Drake, J.C., Peelor, F.F., Biela, L.M., Watkins, M.K., Miller, R.A., Hamilton, K.L., and Miller, B.F. (2013). Assessment of mitochondrial biogenesis and mTORC1 signaling during chronic rapamycin feeding in male and female mice. J. Gerontol. A Biol. Sci. Med. Sci. *68*, 1493–1501.

Eichmann, T.O., Kumari, M., Haas, J.T., Farese, R.V., Jr., Zimmermann, R., Lass, A., and Zechner, R. (2012). Studies on the substrate and stereo/regioselectivity of adipose triglyceride lipase, hormone-sensitive lipase, and diacylglycerol-O-acyltransferases. J. Biol. Chem. *287*, 41446–41457.

Ekstrand, M.I., Falkenberg, M., Rantanen, A., Park, C.B., Gaspari, M., Hultenby, K., Rustin, P., Gustafsson, C.M., and Larsson, N.G. (2004). Mitochondrial transcription factor A regulates mtDNA copy number in mammals. Hum. Mol. Genet. *13*, 935–944.

Erion, D.M., and Shulman, G.I. (2010). Diacylglycerol-mediated insulin resistance. Nat. Med. *16*, 400–402.

Fullerton, M.D., Hakimuddin, F., and Bakovic, M. (2007). Developmental and metabolic effects of disruption of the mouse CTP:phosphoethanolamine cytidylyltransferase gene (Pcyt2). Mol. Cell. Biol. *27*, 3327–3336.

Fullerton, M.D., Hakimuddin, F., Bonen, A., and Bakovic, M. (2009). The development of a metabolic disease phenotype in CTP:phosphoethanolamine cytidylyltransferase-deficient mice. J. Biol. Chem. *284*, 25704–25713.

Funai, K., Song, H., Yin, L., Lodhi, I.J., Wei, X., Yoshino, J., Coleman, T., and Semenkovich, C.F. (2013). Muscle lipogenesis balances insulin sensitivity and strength through calcium signaling. J. Clin. Invest. *123*, 1229–1240.

Griffin, M.E., Marcucci, M.J., Cline, G.W., Bell, K., Barucci, N., Lee, D., Goodyear, L.J., Kraegen, E.W., White, M.F., and Shulman, G.I. (1999). Free fatty acid-induced insulin resistance is associated with activation of protein kinase C theta and alterations in the insulin signaling cascade. Diabetes *48*, 1270–1274.

Hoehn, K.L., Turner, N., Swarbrick, M.M., Wilks, D., Preston, E., Phua, Y., Joshi, H., Furler, S.M., Larance, M., Hegarty, B.D., et al. (2010). Acute or chronic upregulation of mitochondrial fatty acid oxidation has no net effect on whole-body energy expenditure or adiposity. Cell Metab. *11*, 70–76.

Itani, S.I., Ruderman, N.B., Schmieder, F., and Boden, G. (2002). Lipid-induced insulin resistance in human muscle is associated with changes in diacylglycerol, protein kinase C, and IkappaB-alpha. Diabetes *51*, 2005–2011.

Ivanova, P.T., Milne, S.B., Byrne, M.O., Xiang, Y., and Brown, H.A. (2007). Glycerophospholipid identification and quantitation by electrospray ionization mass spectrometry. Methods Enzymol. *432*, 21–57.

Jackowski, S., Wang, J., and Baburina, I. (2000). Activity of the phosphatidylcholine biosynthetic pathway modulates the distribution of fatty acids into glycerolipids in proliferating cells. Biochim. Biophys. Acta *1483*, 301–315.

Kim, J.K., Fillmore, J.J., Sunshine, M.J., Albrecht, B., Higashimori, T., Kim, D.W., Liu, Z.X., Soos, T.J., Cline, G.W., O'Brien, W.R., et al. (2004). PKC-theta knockout mice are protected from fat-induced insulin resistance. J. Clin. Invest. *114*, 823–827.

Kim, M.S., Fielitz, J., McAnally, J., Shelton, J.M., Lemon, D.D., McKinsey, T.A., Richardson, J.A., Bassel-Duby, R., and Olson, E.N. (2008). Protein kinase D1 stimulates MEF2 activity in skeletal muscle and enhances muscle performance. Mol. Cell. Biol. *28*, 3600–3609.

Krank, J., Murphy, R.C., Barkley, R.M., Duchoslav, E., and McAnoy, A. (2007). Qualitative analysis and quantitative assessment of changes in neutral glycerol lipid molecular species within cells. Methods Enzymol. *432*, 1–20.

Lee-Young, R.S., Griffee, S.R., Lynes, S.E., Bracy, D.P., Ayala, J.E., McGuinness, O.P., and Wasserman, D.H. (2009). Skeletal muscle AMP-activated protein kinase is essential for the metabolic response to exercise in vivo. J. Biol. Chem. *284*, 23925–23934.

Leonardi, R., Frank, M.W., Jackson, P.D., Rock, C.O., and Jackowski, S. (2009). Elimination of the CDP-ethanolamine pathway disrupts hepatic lipid homeostasis. J. Biol. Chem. *284*, 27077–27089.

Li, Y., Soos, T.J., Li, X., Wu, J., Degennaro, M., Sun, X., Littman, D.R., Birnbaum, M.J., and Polakiewicz, R.D. (2004). Protein kinase C theta inhibits insulin signaling by phosphorylating IRS1 at Ser(1101). J. Biol. Chem. *279*, 45304–45307.

Lim, H.Y., Wang, W., Wessells, R.J., Ocorr, K., and Bodmer, R. (2011). Phospholipid homeostasis regulates lipid metabolism and cardiac function through SREBP signaling in *Drosophila*. Genes Dev. *25*, 189–200.

Lowry, O.H., and Passonneau, J.V. (1972). A Flexible System of Enzymatic Analysis (Academic Press).

Pavlovic, Z., and Bakovic, M. (2013). Regulation of phosphatidylethanolamine homeostasis — the critical role of CTP:phosphoethanolamine cytidylyltransferase (Pcyt2). Int. J. Mol. Sci. *14*, 2529–2550.

Perseghin, G., Scifo, P., De Cobelli, F., Pagliato, E., Battezzati, A., Arcelloni, C., Vanzulli, A., Testolin, G., Pozza, G., Del Maschio, A., and Luzi, L. (1999). Intramyocellular triglyceride content is a determinant of in vivo insulin resistance in humans: a 1H-13C nuclear magnetic resonance spectroscopy assessment in offspring of type 2 diabetic parents. Diabetes *48*, 1600–1606.

Phielix, E., Meex, R., Ouwens, D.M., Sparks, L., Hoeks, J., Schaart, G., Moonen-Kornips, E., Hesselink, M.K., and Schrauwen, P. (2012). High oxidative capacity due to chronic exercise training attenuates lipid-induced insulin resistance. Diabetes *61*, 2472–2478.

Preiss, J., Loomis, C.R., Bishop, W.R., Stein, R., Niedel, J.E., and Bell, R.M. (1986). Quantitative measurement of sn-1,2-diacylglycerols present in platelets, hepatocytes, and ras- and sis-transformed normal rat kidney cells. J. Biol. Chem. *261*, 8597–8600.

Randle, P.J., Garland, P.B., Hales, C.N., and Newsholme, E.A. (1963). The glucose fatty-acid cycle. Its role in insulin sensitivity and the metabolic disturbances of diabetes mellitus. Lancet *1*, 785–789.

Shindou, H., and Shimizu, T. (2009). Acyl-CoA:lysophospholipid acyltransferases. J. Biol. Chem. *284*, 1–5.

Shindou, H., Hishikawa, D., Harayama, T., Yuki, K., and Shimizu, T. (2009). Recent progress on acyl CoA: lysophospholipid acyltransferase research. J. Lipid Res. *50*, S46–S51.

Srere, P.A. (1969). Citrate synthase. Methods Enzymol. *13*, 3–11.

Sundler, R., Akesson, B., and Nilsson, A. (1974). Quantitative role of base exchange in phosphatidylethanolamine synthesis in isolated rat hepatocytes. FEBS Lett. *43*, 303–307.

Sundram, V., Chauhan, S.C., and Jaggi, M. (2011). Emerging roles of protein kinase D1 in cancer. Mol. Cancer Res. *9*, 985–996.

Tasseva, G., Bai, H.D., Davidescu, M., Haromy, A., Michelakis, E., and Vance, J.E. (2013). Phosphatidylethanolamine deficiency in mammalian mitochondria impairs oxidative phosphorylation and alters mitochondrial morphology. J. Biol. Chem. *288*, 4158–4173.

Turner, N., Kowalski, G.M., Leslie, S.J., Risis, S., Yang, C., Lee-Young, R.S., Babb, J.R., Meikle, P.J., Lancaster, G.I., Henstridge, D.C., et al. (2013). Distinct patterns of tissue-specific lipid accumulation during the induction of insulin resistance in mice by high-fat feeding. Diabetologia *56*, 1638–1648.

Vance, J.E., and Tasseva, G. (2013). Formation and function of phosphatidylserine and phosphatidylethanolamine in mammalian cells. Biochim. Biophys. Acta *1831*, 543–554.

Yu, C., Chen, Y., Cline, G.W., Zhang, D., Zong, H., Wang, Y., Bergeron, R., Kim, J.K., Cushman, S.W., Cooney, G.J., et al. (2002). Mechanism by which fatty acids inhibit insulin activation of insulin receptor substrate-1 (IRS-1)-associated phosphatidylinositol 3-kinase activity in muscle. J. Biol. Chem. *277*, 50230–50236.

Zhu, L., Johnson, C., and Bakovic, M. (2008). Stimulation of the human CTP:phosphoethanolamine cytidylyltransferase gene by early growth response protein 1. J. Lipid Res. *49*, 2197–2211.